

# Parameter ranges for onset of period doubling in the diode resonator

T. L. Carroll, L. M. Pecora

*US Naval Research Lab, Washington, DC 20375*

(July 31, 2002)

## Abstract

One of the classic problems in the study of nonlinear dynamics has been the diode resonator. Previous work with the diode resonator sought to explain the causes of period doubling and chaos, and often used simplified models. This paper instead seeks to link the onset of nonlinear dynamical effects to measurable parameters by comparing experiments and numerical models.

05.45.Gg, 05.45.Vx, 05.45.Xt

## I. INTRODUCTION

Probably the first chaotic electronic circuit to be extensively studied was the diode resonator, consisting of an inductor, a diode, and a resistor, and driven by a periodic signal source [1,2]. The diode itself acts as a nonlinear resistor and a nonlinear charge storage device, so the resulting circuit is a nonlinear resonator with complex dynamics.

Most previous work on the diode resonator is concerned with understanding details of the bifurcations in this circuit or with explaining why such nonlinear effects as period doubling or chaos are present [3–8]. There have been two competing views on the mechanism for period doubling and chaos in the diode resonator: work such as that by Rollins, Hunt and coworkers ( [5] for example) which explain the nonlinear dynamical effects as a result of the "reverse recovery" effect brought on by the exponentially increasing diffusion capacitance, or work along the lines of Matsumoto and collaborators ( [6,7] for example), which model the diode as a piecewise linear capacitance. Both schools of thought find that the diode nonlinear resistance characteristic is not important for the nonlinear dynamics of the diode resonator.

A major problem with both of the above approaches is that in order to make a mathematically tractable model, the researchers must focus on the factors that they consider to be important and remove other effects from their models. Not only do these simplifications lead to models that are not easily described in terms of real physical parameters of the diode, but they encourage circular reasoning. The researchers retain effect  $X$  while neglecting effect  $Y$  and show their model still produces chaos, which they take as proof that  $X$  causes chaos. We do not look for chaos, but among other results, we show below that either one of two commonly considered mechanisms can lead to period doubling.

There have been other papers on nonlinear dynamics in the diode resonator that contain detailed bifurcation diagrams and parameter space plots for a single diode [9,10] . These papers are useful for understanding detailed dynamics of one particular dynamical system, but such a detailed understanding is not our goal here. In this paper, if we are given a

diode and the parameters that are typically available on a commercial datasheet, or easily measurable with simple equipment, and we place that diode in a circuit with an inductor and a resistor, we would like to know if nonlinear dynamical effects will be present for a given periodic driving signal.

The motivation behind this approach is that circuits similar to the diode resonator may be present in complex electronic systems which are designed for audio frequencies, as has been pointed out in [11]. At radio frequencies (rf), wires may act as inductors, producing unintended resonant effects. With the increasing number of radiofrequency signals being broadcast (for example, wireless communications systems are becoming more prevalent), these electronic systems are subject to signals that were never considered when they were designed. It is also possible that an adversary may attempt to interfere with the operation of an electronic system by beaming rf energy towards it.

A circuit designer would then like to know if there is a chance that the circuit will show nonlinear effects such as period doubling when subjected to stray signals. We will work with several different diodes and determine what effect the measurable diode parameters have on the onset of nonlinear dynamical effects.

We intend to scan the drive signal frequency and amplitude over large ranges to look for nonlinear behavior, and to repeat these experiments for a number of different diodes in order to see what effect different physical parameters of the diode have on the onset of nonlinear behavior. In order to cover wide ranges, this scanning must be automated, so we need a marker for nonlinear behavior that is easy to automatically characterize from a time series. We have chosen the onset of the first period doubling as our marker. The first period doubling is very easy to measure automatically, and it is a good indicator that other nonlinear effects may also be likely.

## II. DIODE MODEL

This paper starts with a common technique in which the diode is modeled as a nonlinear resistor in parallel with two nonlinear capacitors [12] (Figure 1). In Figure 1,  $R_N$  represents the nonlinear resistor,  $C_j$  represents the junction capacitance (defined below), and  $C_d$  represents the diffusion capacitance.

The two nonlinear capacitors are used to represent two different charge storage mechanisms in the diode. The junction capacitance refers to the fact that within the depletion region of the diode, there is a stored charge

$$Q_j = A_j \sqrt{V_b - V_a} \quad (1)$$

where  $V_b$  is a barrier voltage characteristic of the diode and  $V_a$  is the voltage drop across the diode.  $A_j$  is a constant that depends on material parameters such as carrier density or lifetime. These parameters may vary considerable within diodes of the same type, so for the purposes of this paper,  $A_j$  is measured from the actual diode (in a later section).

A second charge storage mechanism is diffusion of minority carriers. At the edge of the depletion region, the concentration of minority carriers is high, so minority carriers diffuse into the bulk of the diode. The stored charge,

$$Q_d = A_d e^{\left(\frac{qV_a}{kT}\right)} \quad (2)$$

leads to the diffusion capacitance (which in some models is represented as a "reverse recovery" effect). Once again,  $A_d$  is a constant that depends on material properties. The other constants are  $k$ , the Boltzman constant ( $1.38 \times 10^{-23}$  J/K),  $q$  is the charge of 1 electron ( $1.6 \times 10^{-19}$  C), and  $T$  is the temperature.

Figure 2 is a schematic of a diode resonator, where  $V_0$  is the driving voltage,  $L$  is the inductor (which has a resistance of  $R_L$ )  $V_a$  is the voltage drop across the diode,  $V_C$  is a voltage measured in the experiment, and  $R$  is the resistor. Taking the time derivative of the stored charge leads to an expression for the current through the diode,

$$i = i_R(V_a) + \frac{dQ_j}{dt} + \frac{dQ_d}{dt} = i_R(V_a) + \left[ \frac{-A_j/2}{\sqrt{V_b - V_a}} + \frac{A_d q}{kT} e^{\left(\frac{A_d q}{kT}\right)} \right] \frac{dV_a}{dt} \quad (3)$$

where  $i_R$  is the current through the nonlinear resistor part of the diode. A standard expression for  $i_R$  is [12]

$$i_R(V_a) = I_0 \left( e^{\left(\frac{qV_a}{kT}\right)} - 1 \right) \quad (4)$$

where  $I_0$ , the leakage current, depends on the diode. Equation (3) may be rearranged to give an equation for  $V_a$ :

$$\frac{dV_a}{dt} = -\beta (i - i_R(V_a)) \quad (5)$$

where  $\beta$  is given by

$$\beta = \left\{ \begin{array}{ll} \frac{-\sqrt{V_b - V_a}}{\frac{A_j}{2} - A_d \left(\frac{V_a q}{kT}\right) e^{\left(\frac{V_a q}{kT}\right)} \sqrt{V_b - V_a}} & \text{for } V_a < V_b \\ \frac{1}{A_d \left(\frac{V_a q}{kT}\right) e^{\left(\frac{V_a q}{kT}\right)}} & \text{for } V_a \geq V_b \end{array} \right\} \quad (6)$$

When  $V_a < V_b$ , the diode is in its "off" state, and the nonlinear resistor allows only a small leakage current. When  $V_a > V_b$ , the diode is in its "on" state, and, in the ideal case, the nonlinear resistor may be approximated as a short circuit.

By considering the voltage drops in the circuit, a current equation may be derived:

$$\frac{di}{dt} = \frac{1}{L} (V_a - V_0 + iR) \quad (7)$$

where the resistance  $R$  includes the resistance of the inductor.

### A. Estimating parameters

The parameters  $A_j$ ,  $A_d$ , and  $I_0$  are different for every diode, so it is desirable to measure their values from real diodes. This estimation is not difficult for  $A_j$ .

The constant  $A_j$  may be measured because in reverse bias the diode acts like a capacitor. The diffusion charge term from Eq. (2) is very small for reverse bias ( $V_a < 0$ ), so essentially all of the diode capacitance comes from the junction charge. Taking the derivative of Eq. (1) with respect to voltage gives

$$C_j(V_a) = -\frac{dQ_j}{dV_a} = \frac{\left(\frac{1}{2}\right) A_j}{\sqrt{V_b - V_a}} = \frac{0.5A_j/\sqrt{V_b}}{\sqrt{1 - V_a/V_b}} \quad (8)$$

so that if  $C_j(0)$  is the junction capacitance for  $V_a = 0$  V, then  $A_j = 2\sqrt{V_b}C_j(0)$ .

The diode capacitance may be measured easily if one makes the diode part of a high pass filter, as shown in Figure 3. The voltage  $V_0$  is the sum of a steady part and a time varying part:

$$V_0(t) = D_0 + D_1 \sin(2\pi ft) \quad (9)$$

where  $D_1$  was 50 mV. From Eq. (8), as  $D_0$  varies, the capacitance of the diode should also vary.

The magnitude of the transfer function for a first order high pass filter is [13]

$$|A(f)| = \frac{1}{\sqrt{1 + 1/(2\pi f RC)^2}} \quad (10)$$

where  $C$  in this case is  $C_j(V_a)$ , and  $V_a$  is the voltage drop across the diode. For a value of  $R = 1M\Omega$ , the magnitude of the transfer function was measured as a function of frequency and fit to the curve of Eq.(10) by varying  $C$ . This process is repeated for different values of  $D_0$  to produce a curve of capacitance as a function of  $D_0$ .

There is some offset in the measurement circuit caused by its own capacitance, so this is accounted for by fitting the capacitance curve by the function of Eq. (8) but with an added offset. We find that the measurement circuit adds an offset of 17 pF. The curve of diode capacitance as a function of  $D_0$  for an mv2101 diode before subtracting the offset is shown in Figure 4. For this diode,  $C_j(0)$  is 17 pF.

In principle, it should also be possible to estimate  $A_d$  from the actual diode, but the diffusion charge is an exponential function of  $V_a$ , so in practice this measurement is not possible.  $A_d$  is instead estimated from measurements of diode recovery time, discussed below.

The leakage current  $I_0$  (the current that flows in reverse bias) could be measured, but this current is on the order of nanoamps, requiring sophisticated measurement apparatus, so instead typical values from diode data sheets are used.

### III. REVERSE RECOVERY

As mentioned above, if  $V_a$  is quickly switched from a value above  $V_b$  to a value below zero, the diffusion charge flows out as a reverse recovery current. In order to measure the reverse recovery, the diode is placed in series with a 1 k $\Omega$  resistor to ground and driven with a square wave, as in Figure 5. Figure 6 shows time series traces for  $V_0$  (the driving voltage) and  $V_c$  (the voltage drop across the fixed resistor  $R$ ) for an mv2101 diode. When  $V_0$  drops to zero,  $V_c$  is still nonzero for a time known as the reverse recovery time because of the flow of diffusion charge. The reverse recovery time actually varies as the height or width of the  $V_0$  pulse varies, but for large pulses the reverse recovery time saturates. When a reverse recovery time is given in this paper, it is the saturation value. For the circuit shown, the reverse recovery time is 0.88  $\mu$ s.

The reverse recovery effect may be simulated from the diode equations. Since there is no inductor, only one differential equation is needed:

$$\frac{dV_a}{dt} = -\beta (i - i_R(V_a)) \quad (11)$$

where  $I_R(V_a)$  is given by Eq. (4),  $\beta$  is given by Eq. (6) and  $i = (V_0 - V_a)/R$ . At room temperature, the factor of  $q/kT$  in Eq. (4) is approximately 38 V<sup>-1</sup>. Because Eq. (4) contains an exponential of a large number, the diode equations are stiff, so in order to numerically integrate them a stiff solver was used [14].

Figure 7 shows time series of  $V_0$  (dotted line) and  $V_a$  (solid line) from a simulation of Eq. (11) with parameters  $A_j = 17 \times 10^{-12}$  FV<sup>1/2</sup> (Farads  $\times$  Volts<sup>1/2</sup>),  $I_0 = 2 \times 10^{-11}$  A (Amps) (a typical value from a datasheet for a mv2101 diode),  $R = 1$  k $\Omega$ ,  $V_b = 0.6$  V (Volts) (the value for an mv2101 diode) and  $A_d = -1 \times 10^{-18}$  C (Coulombs). The last constant,  $A_d$ , was difficult to estimate from the actual diode, so its value was adjusted to vary the reverse relaxation time. In Fig 7(a),  $V_0$  varied between 0 and 1 V, resulting in a reverse recovery time of 37 ns, while in 7(b)  $V_0$  varied from 0 to 5 V, giving a reverse recovery time of 116 ns, which is approximately the saturation value for this simulation. Larger values of  $A_d$  or smaller values of  $I_0$  led to longer relaxation times.

## IV. PERIOD DOUBLING

### A. Experiment

The goal of this paper is to determine for what parameter regions nonlinear effects will occur in the diode resonator. As we state above, we would like to scan drive frequency and amplitude for a number of different diodes, so we need an indicator of nonlinear behavior that is easy to measure from a time series. We choose the onset of the first period doubling as our marker because it is easy to automatically recognize from a time series.

A number of different diodes and circuit elements were used with the diode resonator circuit of Fig. 1 in the search for the onset of period doubling. Table I contains a list of circuit parameters. The resistor  $R$  was  $100 \Omega$  for each plot. Once again,  $V_0$  was given by

$$V_0(t) = D_0 + D_1 \sin(2\pi ft) \quad (12)$$

where  $D_0 = 0$ , and  $D_1$  and  $f$  could be varied. For each combination of  $D_1$  and  $f$ , a time series of  $V_c$  was digitized and the power spectrum was calculated. The power at  $f/2$  was measured, and this number was divided by the average power between frequencies of 0 and  $f$ . Figure 8 shows the regions (in black) where the half frequency peak exceeds twice the average power for the diode resonators listed in Table I. The period doubling onset corresponds to the border of the black regions. The horizontal axes in Fig. 8 are  $f_n = f/f_0$ , where  $f_0 = 1/(2\pi\sqrt{LC_j(0)})$  is the resonant frequency of the series  $LRC$  circuit with a capacitance of  $C_j(0)$ , while the vertical axes in Fig 8 are the driving amplitude  $D_1$ . These plots are for several different diodes with different junction capacitances and reverse recovery times, and different inductors, but the period doubling onset always occurs for the same range of  $f_n$ , that is for  $f_n$  roughly between 0.25 and 2. This same pattern was seen for driving frequencies as high as 50 MHz, which was the upper limit of the equipment in our lab ( $f_0$  in that case was 32 MHz).

There were 2 diodes for which period doubling was not seen, a 1n4148 and a 1n4100. The 1n4148 was a fast recovery diode with a junction capacitance  $C_j(0) < 2$  pF (too small to

be measured by the technique described above), while the 1n4100 had a measured junction capacitance of 949 pF. It was difficult to measure a reverse recovery time in the 1n4100 because of the large junction capacitance.

The most likely reason that period doubling was not observed in the 1n4148 diode was because stray capacitance in the breadboard used to construct the diode resonator was larger than the junction capacitance of the diode. Experiments with a 1n4383 diode with  $C_j(0) = 70$  pF showed that adding a 70 pF capacitor in parallel with the diode completely suppressed the period doubling. The stray capacitance in the breadboard was approximately 17 pF, much larger than  $C_j(0)$  for the 1n4148 diode, so period doubling was probably suppressed by this stray capacitance. Possible reasons why period doubling was not seen in the 1n4100 diode are explored in the simulations below.

## B. Simulations

The diode resonator was simulated by integrating Eqs. (5 - 7) with a stiff solver [14]. Figure 9 shows the ratio of the half frequency power to the average power (black is the largest ratio) for the model of the diode resonator with different parameter values, given by Table II (for all plots,  $L = 68$  mH,  $A_j = 17 \times 10^{-12}$  FV<sup>1/2</sup>,  $f_0 = 184$  kHz). The onset of period doubling still occurs in roughly the same range of  $f_n$  as it did in the experiment, so the model appears to be useful in predicting the behavior of a real diode resonator. It appears that  $A_d$  and  $I_0$  by themselves have no direct effect on the period doubling onset (the border of the shaded regions), but they affect the dynamics by their effect on the reverse recovery time  $T_{rr}$ . Smaller values of  $T_{rr}$  do not seem to have much effect on the period doubling onset, but large values of  $T_{rr}$  do appear to broaden the range of period doubling. Figure 10 is a plot of the period doubling region for  $A_d = 0$  ( $A_j = 17 \times 10^{-12}$  FV<sup>1/2</sup>,  $I_0 = 2 \times 10^{-12}$  A,  $L = 68$  mH) so that  $T_{rr} = 0$ . Period doubling still occurs for  $T_{rr} = 0$ . Some models of the diode resonator use only the reverse recovery effect to produce nonlinear dynamical effects [3,5], but reverse recovery is not necessary to cause period doubling in this model.

We may also consider the opposite situation in which the diffusion capacitance is the variable part of the diode capacitance while the junction capacitance is set to a constant. In this case, the term  $\beta$  in Eq. (6) becomes

$$\beta = \frac{1}{A_d \left( \frac{V_{a0}}{kT} \right) e^{\left( \frac{V_{a0}}{kT} \right)} - \frac{A_j \sqrt{V_b}}{2}} \quad (13)$$

Figure 11 is a plot of the resulting period doubling region for  $A_d = -1 \times 10^{-18} \text{ C}$  ,  $A_j = 17 \times 10^{-12} \text{ FV}^{1/2}$  ,  $I_0 = 2 \times 10^{-12} \text{ A}$  ,  $L = 1 \text{ mH}$ . Once again, period doubling onset is seen for substantially the same region of normalized frequency as before. What is clear from Figs. 10 and 11 is that while a rise in capacitance as the diode forward bias voltage increases is sufficient to cause period doubling, the model used in this work can not distinguish whether this rise is caused by the diffusion capacitance or the junction capacitance. The shape of the period doubling regions on the plots in Figs. 9-11 is most like the regions seen in the experimental plots of Fig. 8 when both junction and diffusion capacitance were present. In a real diode, it is not possible to set diffusion capacitance to 0 or to set junction capacitance to a constant, so it is probably not very accurate to say that one type of capacitance or the other is the sole cause of the period doubling.

The reverse recovery effect actually appears to suppress period doubling if  $T_{rr}$  is too long compared to  $1/f_0$  . Figure 12 shows a series of plots from the model for which  $T_{rr}$  was fixed at  $1.2 \times 10^{-7} \text{ s}$  ( $A_d = -1 \times 10^{-18} \text{ C}$  ,  $I_0 = 2 \times 10^{-11} \text{ A}$  ,  $A_j = 17 \times 10^{-12} \text{ FV}^{1/2}$ ) but  $f_0$  was increased by decreasing the value of the inductor  $L$ . For Fig. 12(a),  $L = 50 \text{ mH}$  ( $f_0 = 214 \text{ kHz}$ ), for (b)  $L = 0.5 \text{ mH}$  ( $f_0 = 2.14 \text{ MHz}$ ), for (c)  $L = 5 \text{ } \mu\text{H}$  ( $f_0 = 21.4 \text{ MHz}$ ), and for (d)  $L = 0.05 \text{ } \mu\text{H}$  ( $f_0 = 214 \text{ MHz}$ ). For the largest value of  $f_0$  period doubling was suppressed. If  $T_{rr}$  was smaller, then period doubling was not suppressed until higher driving frequencies. Unfortunately, a signal source with enough power (at high frequencies) to measure this suppression in a real diode was not available. The important consequence for a circuit designer would be to use a diode with the longest recovery time practical in order to avoid period doubling.

There is still the question of why period doubling was not seen in a 1n4100 diode, which

had a large junction capacitance ( $C_j(0) = 949$  pF). The effect of large junction capacitance on the diode resonator model was studied by fixing  $A_d = -1 \times 10^{-18}$  C,  $I_0 = 2 \times 10^{-11}$  A,  $L = 1$  mH (other parameters as before) and increasing  $A_j$ . Figure 13(a) is the period doubling region for  $A_j = 17 \times 10^{-12}$  FV<sup>1/2</sup> ( $f_0 = 1.5$  MHz), (b) is for  $A_j = 17 \times 10^{-10}$  ( $f_0 = 150$  kHz), and 13(c) is for  $A_j = 17 \times 10^{-8}$  ( $f_0 = 15$  kHz). Period doubling is suppressed for the largest value of  $A_j$ , although this corresponds to  $C_j(0) = 1.1 \times 10^{-7}$  F, which is much larger than the value of  $9.49 \times 10^{-10}$  F measured for the 1n4100 diode.

The suppression of period doubling was caused by the large values of  $A_j$  and not by the low values of  $f_0$ ; low values of  $f_0$  were also obtained by holding  $A_j$  fixed at  $17 \times 10^{-12}$  FV<sup>1/2</sup> and increasing the inductor  $L$ , but no suppression of period doubling was seen in this case. In an experiment with an mv2101 diode ( $C_j(0) = 17$  pF), period doubling was not suppressed when  $f_0$  was as low as 3.3 kHz.

## V. CONCLUSIONS

It is possible to predict the presence of period doubling in the diode resonator from a few measurable diode parameters. The most important parameter is junction capacitance—if period doubling occurs, it will occur within a range of  $0.25f_0$  to  $2f_0$ , where  $f_r = 1/(2\pi\sqrt{LC_j(0)})$ . Diffusion capacitance in the diode causes the reverse recovery effect, which was considered to be the cause of period doubling in some models, but here is only important because reverse recovery times that are long compared to  $1/f_0$  suppress period doubling, while period doubling is still present for a reverse recovery time of 0. In addition, very large junction capacitances can also suppress period doubling. At low frequencies, the model agrees well with experiments, although the experiments could not be extended to high enough frequencies to confirm all aspects of the model.

## REFERENCES

- [1] P. S. Linsay, *Physical Review Letters* **47**, 1349-1352 (1981)
- [2] J. Testa, J. Perez and C. Jeffries, *Physical Review Letters* **48**, 714-717 (1982)
- [3] E. R. Hunt and R. W. Rollins, *Physical Review A* **29**, 1000-1002 (1984)
- [4] C. M. Kim, C. H. Cho, C. S. Lee, J. H. Yim, J. Kim, Y. Kim, *Physical Review A* **38**, 1645-1648 (1988)
- [5] Z. Su, R. W. Rollins and E. R. Hunt, *Physical Review A* **40**, 2698-2705 (1989)
- [6] N. Takeuchi, T. Nagai and T. Matsumoto, *Electronics and Communications in Japan* **84**, 91-99 (2001)
- [7] S. Tanaka, S. I. Higuchi and T. Matsumoto, *Physical Review E* **54**, 6014-6028 (1996)
- [8] J. M. Perez, *Phys. Rev. A* **32**, 2513-2516 (1985)
- [9] T. Klinker, W. Meyer-Ilse, W. Lauterborn, *Phys. Lett. A* **101A**, 371-375 (1984)
- [10] S. D. Brorson, D. Dewey, P. S. Linsay, *Phys. Rev. A* **28**, 1201-1203 (1983)
- [11] V. I. Ponomarenko, M. D. Prokhorov and Y. P. Seleznev, *Low-dimensional model of a microwave resonator with a p-n junction varactor*, IEEE-Russia Conference on High Power Microwave Electronics: Measurements, Identification, Applications, Novosibirsk, Russia, 1999, (IEEE)
- [12] M. J. Cooke, *Semiconductor Devices* (Prentice Hall, Englewood Cliffs, 1990)
- [13] U. Tietze and C. Shenk, *Electronic Circuits* (Springer, Berlin, 1991)
- [14] W. H. Press, B. P. Flannery, S. A. Teukolsky and W. T. Vetterling, *Numerical Recipes* (Cambridge University Press, New York, 1990)

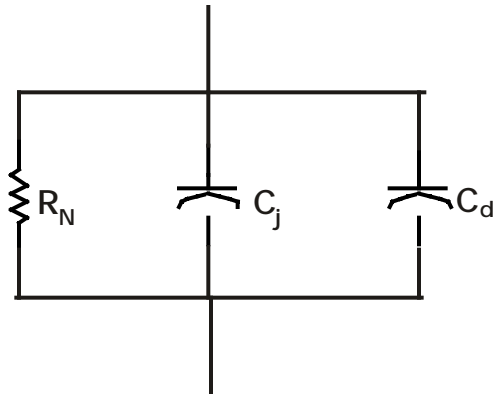


Figure 1. Simple representation of a common model for a diode, where  $R_N$  is a nonlinear resistance,  $C_j$  is the junction capacitance, and  $C_d$  is the diffusion capacitance.

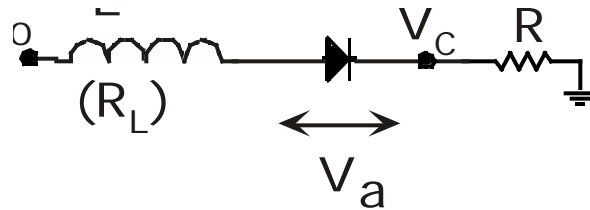


Figure 2. Schematic of a diode resonator circuit, consisting of an inductor  $L$  (which has a dc resistance of  $R_L$ ), a diode (the black arrow-like object), and a resistor  $R$ . The diode resonator is driven by the voltage  $V_0$ , and in the experiment the measured signal is  $V_C$ .  $V_a$  is the voltage drop across the diode, which is modeled in the simulations.

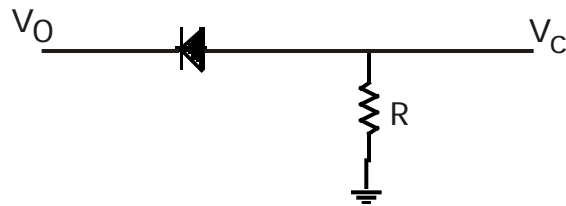


Figure 3. Circuit used to measure the diode capacitance.  $R$  is a 1 M resistor.

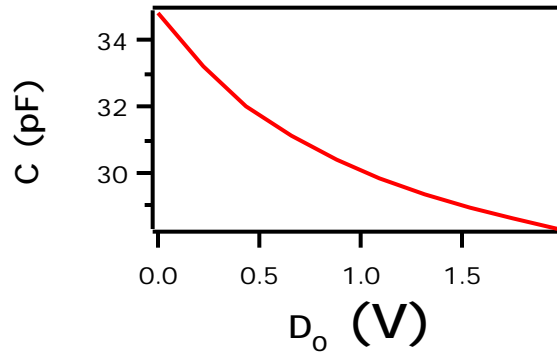


Figure 4. Measured capacitance  $C$  as a function of bias voltage  $D_0$  for an mv2101 diode. The capacitance value is offset by 17 pF because of the capacitance of the measurement apparatus.

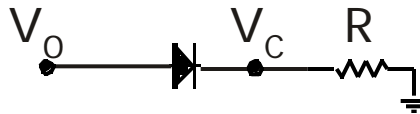


Figure 5. Circuit used to measure the diode reverse recovery time.  $R$  was a 1 k  $\Omega$  resistor.

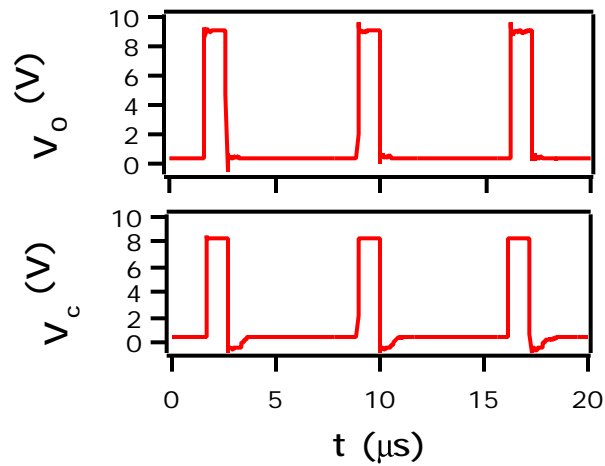


Figure 6. The top trace is the driving signal  $V_0$  applied to the circuit of Fig. 5, while the bottom trace is the measured signal  $V_C$ . When  $V_0$  goes to 0,  $V_C$  goes to -0.6 V for a short time because of the reverse recovery effect.

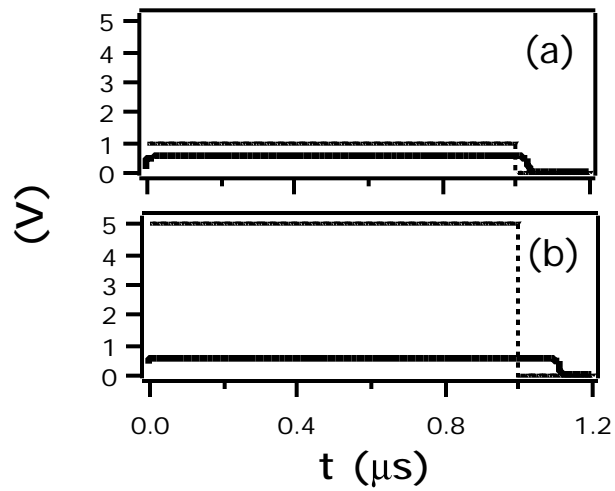


Figure 7. Simulation of the reverse recovery effect.  $V_0$ , the driving signal, is a dotted line, while the solid line is  $V_a$ , the voltage drop across the diode. The parameters were  $A_d = 17 \times 10^{-12} \text{ FV}^{1/2}$ ,  $I_0 = 2 \times 10^{-11} \text{ A}$ ,  $R = 1 \text{ k}$ ,  $V_b = 0.6 \text{ V}$  and  $A_j = 1 \times 10^{-18} \text{ C}$ . In (a),  $V_0$  varied between 0 and 1 V, resulting in a reverse recovery time of 37 ns, while in (b)  $V_0$  varied between 0 and 5 V, so that the reverse recovery time was 116 ns.

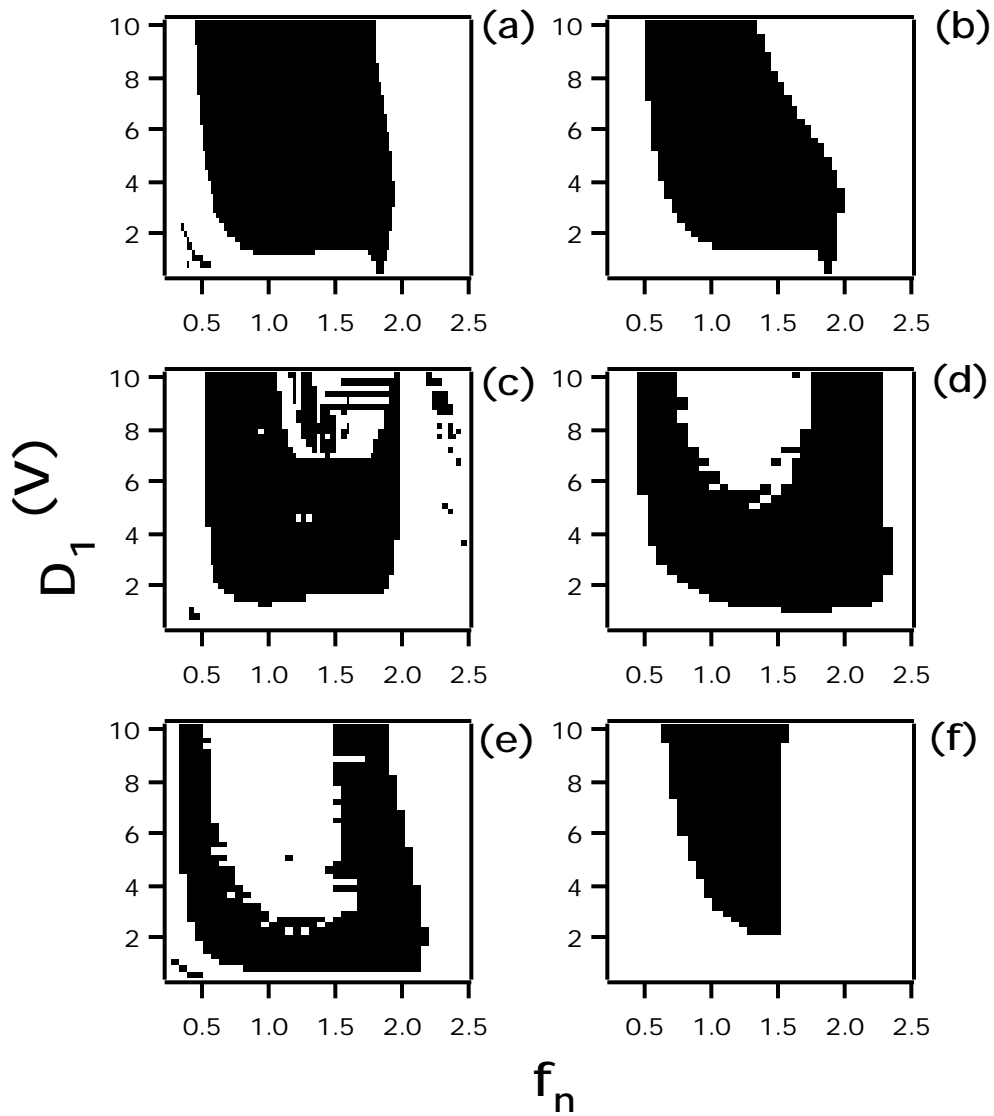


Figure 8. Onset of period doubling for the diode resonator experiment using several different diodes (period doubling region in black). The key to the figure is in table I. The frequency  $f_n$  has been normalized so that  $f_n = 1$  corresponds to the resonant frequency of the diode resonator at 0 bias voltage.

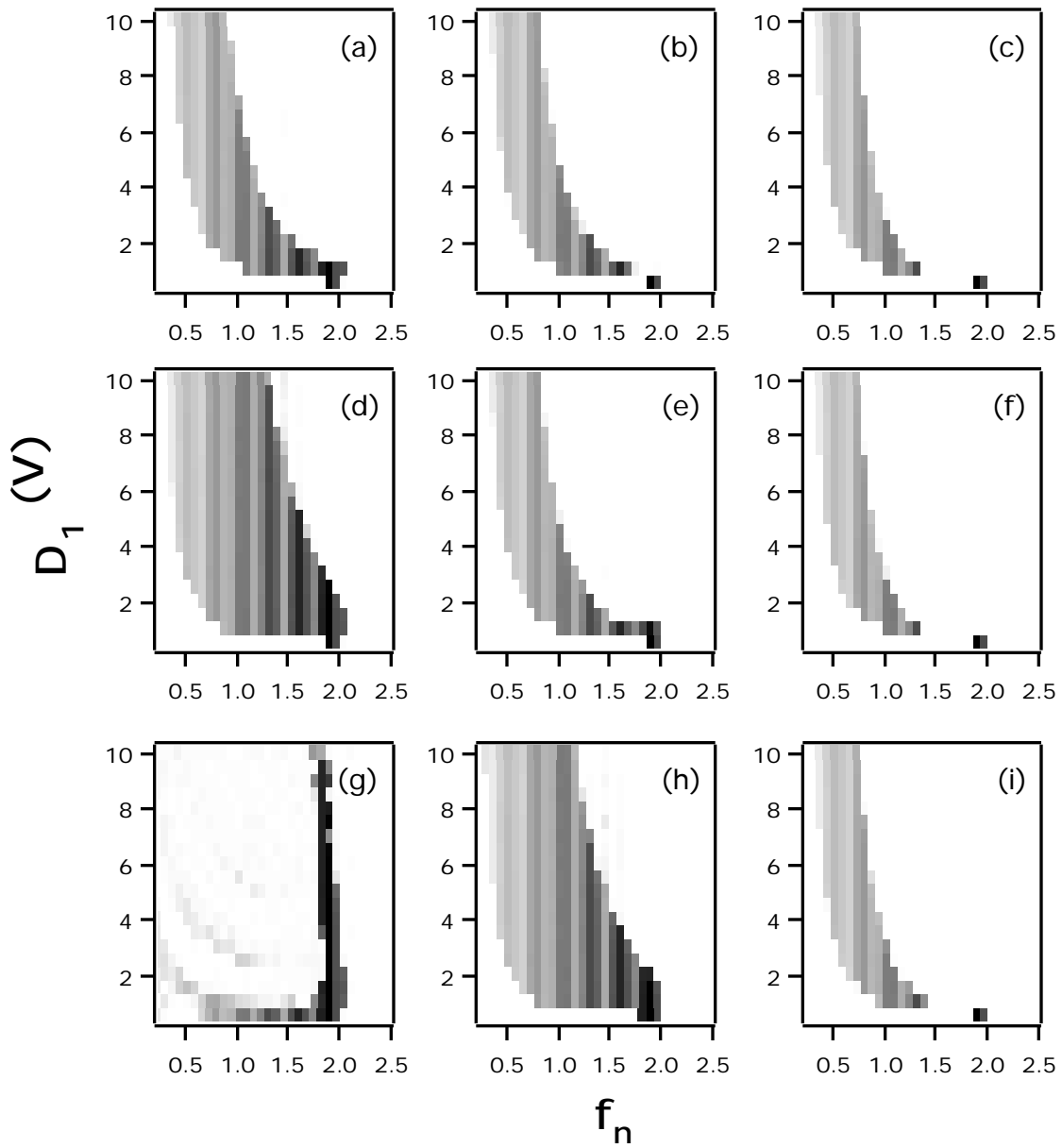


Figure 9. Onset of period doubling for the model of the diode resonator , with  $A_j = 17 \times 10^{-12} \text{ FV}^{1/2}$  ,  $L = 68 \text{ mH}$ , and the other parameters varying according to table II. The grayscale shows the ratio of the half frequency power to the average power (between dc and the driving signal) in the simulated version of  $V_a$  , with black representing the largest value. The frequency  $f_n$  has been normalized so that  $f_n = 1$  corresponds to the resonant frequency of the diode resonator at 0 bias voltage.

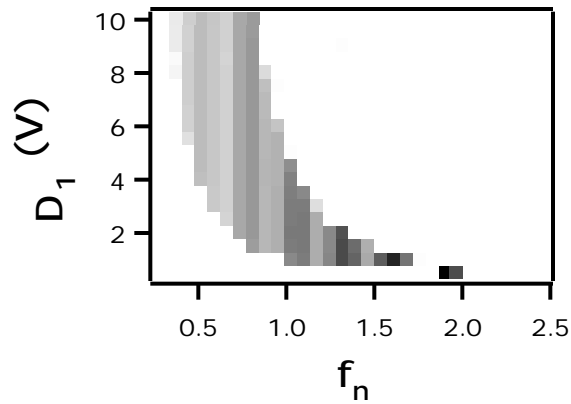


Figure 10. Period doubling onset for the diode resonator model with a reverse recovery time  $T_{rr} = 0$ . The parameters were  $A_d = 0$ ,  $A_j = 17 \times 10^{-12} \text{ FV}^{1/2}$ ,  $I_0 = 2 \times 10^{-12} \text{ A}$ . The grayscale shows the ratio of the half frequency power to the average power (between dc and the driving signal) in the simulated version of  $V_a$ , with black representing the largest value. The frequency  $f_n$  has been normalized so that  $f_n = 1$  corresponds to the resonant frequency of the diode resonator at 0 bias voltage.

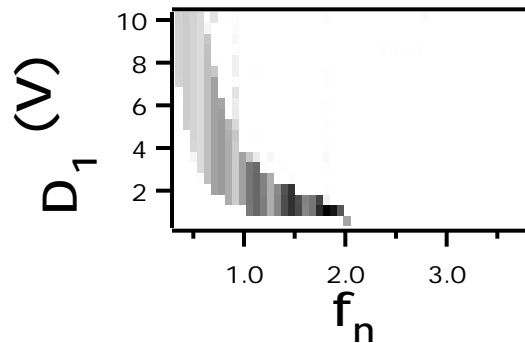


Figure 11. Period doubling onset for the numerical model of the diode resonator when the junction capacitance is constant. The parameters for this plot were  $A_d = -1 \times 10^{-18} \text{ C}$ ,  $A_j = 17 \times 10^{-12} \text{ FV}^{1/2}$ ,  $I_0 = 2 \times 10^{-12} \text{ A}$ ,  $L = 1 \text{ mH}$ . The frequency  $f_n$  has been normalized so that  $f_n = 1$  corresponds to the resonant frequency of the diode resonator at 0 bias voltage.

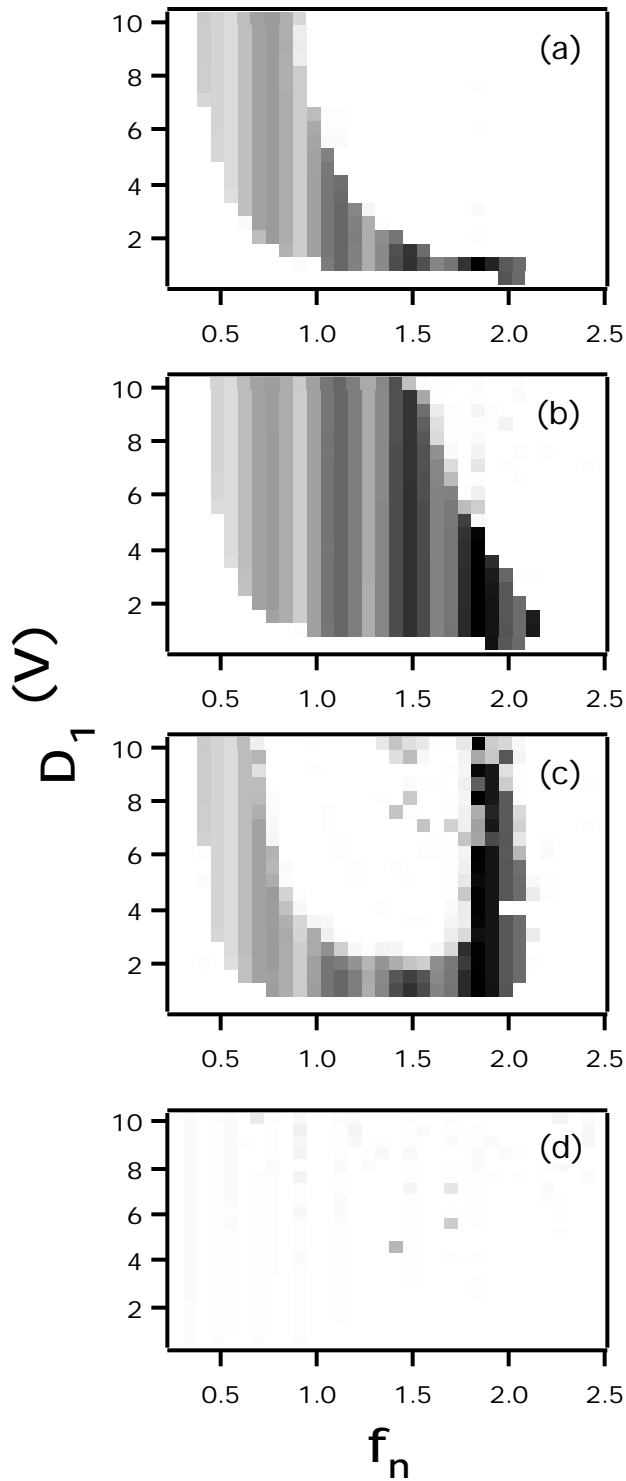


Figure 12. In these plots from the model,  $T_r$  is fixed at  $1.2 \times 10^{-7}$  s, but the resonant frequency  $f_0$  is increased by increasing the inductor value. These plots are intended to show how the reverse recovery time affects the period doubling region at different resonant frequencies. (a),  $L = 50$  mH ( $f_0 = 302$  kHz), for (b)  $L = 0.5$  mH ( $f_0 = 3.02$  MHz),

for (c)  $L = 5 \mu\text{H}$  ( $f_0 = 30.2 \text{ MHz}$ ), and for (d)  $L = 0.05 \mu\text{H}$  ( $f_0 = 300.2 \text{ MHz}$ ). The grayscale shows the ratio of the half frequency power to the average power (between dc and the driving signal) in the simulated version of  $V_a$ , with black representing the largest value. The frequency  $f_n$  has been normalized so that  $f_n = 1$  corresponds to the resonant frequency of the diode resonator at 0 bias voltage.

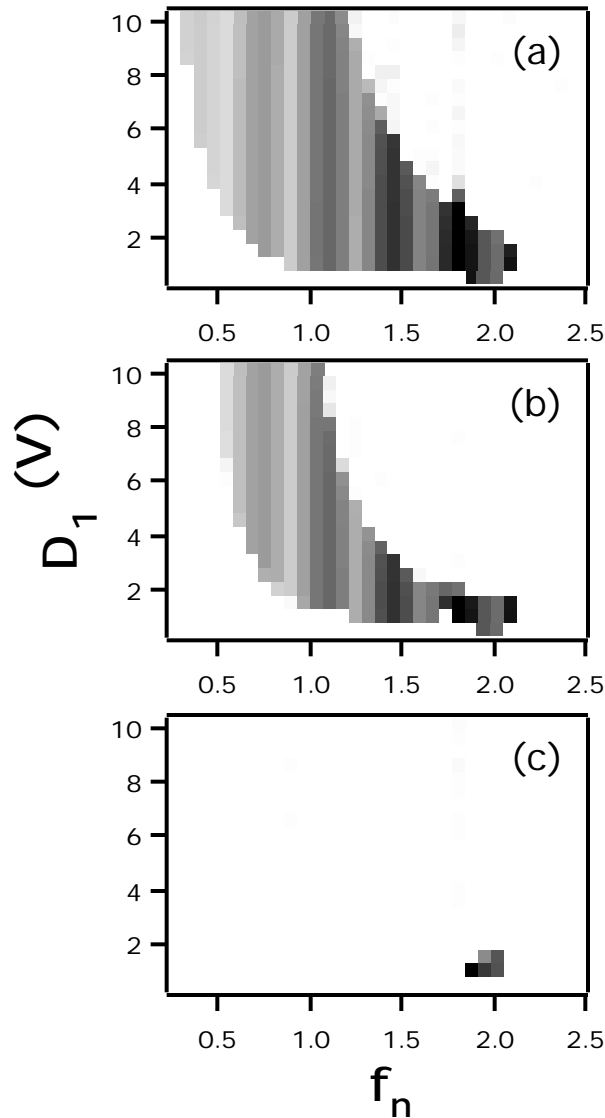


Figure 13. These plots from the model show how large values for the junction capacitance  $C_j$  (which is proportional to  $A_j$ ) affect period doubling. The fixed parameters were  $A_d = -1 \times 10^{-18} \text{ C}$ ,  $I_0 = 2 \times 10^{-11} \text{ A}$ ,  $L = 1 \text{ mH}$ , while for (a)  $A_j = 17 \times 10^{-12} \text{ FV}^{1/2}$  ( $f_0 = 9.5 \text{ MHz}$ ), (b) is for  $A_j = 17 \times 10^{-10} \text{ FV}^{1/2}$  ( $f_0 = 950 \text{ kHz}$ ), and (c) is for  $A_j = 17 \times 10^{-8} \text{ FV}^{1/2}$  ( $f_0 = 95 \text{ kHz}$ ). The grayscale shows the ratio of the half frequency power to the average power (between dc and the driving signal) in the simulated version of  $V_a$ , with black representing the largest value. The frequency  $f_n$  has been normalized so that  $f_n = 1$  corresponds to the resonant frequency of the diode resonator at 0 bias voltage.

TABLES

TABLE I. Parameters for the plots of Fig. 8 (from the experimental diode resonator circuit)

| plot | diode  | $L$ (mH) | $R_L$ ( $\Omega$ ) | $C_j$ (pF) | $T_{rr}$ $\mu$ S | $1/\sqrt{LC_j}$ |
|------|--------|----------|--------------------|------------|------------------|-----------------|
| (a)  | mv2101 | 10       | 100                | 17         | 0.88             | 386 kHz         |
| (b)  | mv2101 | 68       | 539                | 17         | 0.88             | 148 kHz         |
| (c)  | mv2101 | 1        | 59                 | 17         | 0.88             | 1.22 MHz        |
| (d)  | 1n4385 | 68       | 539                | 99         | 0.18             | 0.61 MHz        |
| (e)  | 1n4383 | 68       | 539                | 24         | 0.04             | 0.78 MHz        |
| (f)  | 1n4383 | 68       | 539                | 70         | 0.09             | 73 kHz          |

TABLE II. Parameters for the plots of Fig. 9 (from simulations of the diode resonator circuit).

|     | $I_0$ (A)           | $A_d$ (C)            | $T_{rr}$ (s)         |
|-----|---------------------|----------------------|----------------------|
| (a) | $2 \times 10^{-12}$ | $-1 \times 10^{-19}$ | $1.1 \times 10^{-7}$ |
| (b) | $2 \times 10^{-11}$ | $-1 \times 10^{-19}$ | $1.6 \times 10^{-8}$ |
| (c) | $2 \times 10^{-10}$ | $-1 \times 10^{-19}$ | $4 \times 10^{-9}$   |
| (d) | $2 \times 10^{-12}$ | $-1 \times 10^{-18}$ | $1 \times 10^{-6}$   |
| (e) | $2 \times 10^{-11}$ | $-1 \times 10^{-18}$ | $1.2 \times 10^{-7}$ |
| (f) | $2 \times 10^{-10}$ | $-1 \times 10^{-18}$ | $1.5 \times 10^{-8}$ |
| (g) | $2 \times 10^{-12}$ | $-1 \times 10^{-17}$ | $1 \times 10^{-5}$   |
| (h) | $2 \times 10^{-11}$ | $-1 \times 10^{-17}$ | $1.1 \times 10^{-6}$ |
| (i) | $2 \times 10^{-10}$ | $-1 \times 10^{-17}$ | $1.2 \times 10^{-7}$ |